ROSAT PSPC and HRI observations of the composite starburst/Seyfert 2 galaxy NGC 1672

W.N. Brandt,[1] J.P. Halpern[2] and K. Iwasawa[1]

[1] *Institute of Astronomy, Madingley Road, Cambridge CB3 0HA (Internet: wnb@ast.cam.ac.uk, ki@ast.cam.ac.uk)*
[2] *Columbia Astrophysics Laboratory, Columbia University, 538 West 120th Street, New York, NY 10027 USA (Internet: jules@carmen.phys.columbia.edu)*

ABSTRACT

The nearby barred spiral galaxy NGC 1672 has been observed with the Position Sensitive Proportional Counter (PSPC) and High Resolution Imager (HRI) instruments on board the *ROSAT* X-ray satellite. NGC 1672 is thought to have an obscured Seyfert nucleus, and it has strong starburst activity as well. Three bright X-ray sources with luminosities $1\text{–}2\times10^{40}$ erg s^{-1} are clearly identified with NGC 1672. The strongest lies at the nucleus, and the other two lie at the ends of NGC 1672's prominent bar, locations that are also bright in Hα and near-infrared images. The nuclear source is resolved by the HRI on about the scale of the recently identified nuclear ring, and one of the sources at the ends of the bar is also probably resolved. The X-ray spectrum of the nuclear source is quite soft, having a Raymond-Smith plasma temperature of ≈ 0.7 keV and little evidence for intrinsic absorption. The *ROSAT* band X-ray flux of the nuclear source appears to be dominated not by X-ray binary emission but rather by diffuse gas emission. The absorption and emission properties of the sources, as well as their spatial extents, lead us to models of superbubbles driven by supernovae. However, the large density and emission measure of the nuclear X-ray source stretch the limits that can be comfortably accommodated by these models. We do not detect direct emission from the putative Seyfert nucleus, although an alternative model for the nuclear source is thermal emission from gas that is photoionized by a hidden Seyfert nucleus. The spectra of the other two X-ray sources are harder than that of the nuclear source, and have similar difficulties with regard to superbubble models.

Key words: galaxies: individual: NGC 1672 – galaxies: individual: NGC 1688 – galaxies: Seyfert – X-rays: galaxies.

1 INTRODUCTION

1.1 Basic facts

NGC 1672 (PKS 0444 − 593) is a $V = 10.1$ barred spiral galaxy of type SB(s)b. It is the principal galaxy in a group that is partially covered by the Large Magellanic Cloud, and a member of the Dorado cloud complex (see fig. 4 of de Vaucouleurs 1975). The radial velocity of NGC 1672 relative to the centroid of the Local Group is 1 140 km s^{-1} (Osmer, Smith & Weedman 1974; hereafter OSW74). It has *four* principal outer arms and these contain many H II regions 2–4 arcsec in size (Sandage & Bedke 1994). On deep optical photographs the arms can be seen to extend out to about 6 arcmin from NGC 1672's centre, although they become quite faint outside about 3 arcmin from the centre (cf. Sandage & Bedke 1994). Its bar has a length of 2.4 arcmin and vigorous star formation is seen at its ends (Baumgart & Peterson 1986), as is consistent with theoretical calculations of density enhancements associated with bars (see sect. 9 of Athanassoula 1992 and references therein). Conspicuous dust lanes are present along the leading edges of the bar (Baumgart & Peterson 1986). Elmegreen et al. (1991) suggested that NGC 1672 may have interacted with NGC 1688 and that this interaction may have led to NGC 1672's 'ocular' central shape. The centres of NGC 1672 and NGC 1688 are separated by 39 arcmin, and NGC 1688 is roughly one third as massive as NGC 1672. We shall adopt a Hubble constant of $H_0 = 50$ km s^{-1} Mpc^{-1} and a cosmological deceleration parameter of $q_0 = \frac{1}{2}$ throughout. This gives a distance to NGC 1672 of 22.8 Mpc (assuming the proper motion of NGC 1672 is small relative to its Hubble flow velocity). At this distance NGC 1672's bar is 16 kpc long and the HRI's spatial resolution (≈ 5 arcsec) corresponds to about 550 pc.

1.2 The nuclear region

The nucleus of NGC 1672 was noted to be peculiar by Sérsic & Pastoriza (1965). Pastoriza (1973) stated that it has dimensions of $\approx 22 \times 14$ arcsec with its longest axis lying in the Northeast direction. An isophotal map of the nuclear region can be found in Sérsic (1968). The nuclear spectrum has a polarization of ≤ 1.2 per cent in the B, R and H bands (Brindle et al. 1990). The relative strengths of the optical

emission lines in the spectrum taken through a 20 arcsec aperture are similar to those found in ordinary H II regions (OSW74), although sources of gas ionization in addition to normal OB stars cannot be ruled out. Storchi-Bergmann, Wilson & Baldwin (1996; hereafter SWB96) classified the nuclear spectrum as a LINER, although the details of spatially resolved emission-line profiles and ratios in the inner 2 arcsec have also been interpreted as evidence of a composite spectrum of a Seyfert nucleus and H II regions, as described below. NGC 1672 does not have a 'warm' IRAS colour in the sense of Sanders et al. (1988).

The manifestations of Seyfert activity in the centre of NGC 1672 are the following:

1. Optical spectra of the nucleus of NGC 1672 in a 2×4 arcsec aperture show that its [O III] lines have FWHM ≈ 300 km s^{-1} while its Hβ line has a FWHM of only 150 km s^{-1} (Véron, Véron & Zuiderwijk 1981). These authors argued that the presence of [O III] broader than Hβ is the signature of a composite Seyfert 2/H II region spectrum, in which the [O III] emission comes primarily from a Seyfert nucleus whose [O III]/Hβ ratio is large. The Hβ flux then comes primarily from a region of circumnuclear starburst activity, where there [O III]/Hβ ratio is small (if there is a broad-line region associated with the postulated Seyfert nucleus it must be either intrinsically very weak or obscured; note from Figure 1 the requisite tilted obscuration geometry relative to NGC 1672's disc). Díaz (1985) and García-Vargas et al. (1990) presented spatially resolved spectroscopy of NGC 1672 which shows a strong increase in the [O III] line strength near the nucleus. In the very central region (1.3×1.6 arcsec) [O III]/H$\beta \approx 1$ while away from this region [O III]/Hβ is significantly less than unity. Their spectra reveal that in the very central region both [O III] and Hβ have about the same FWHM of ≈ 300 km s^{-1}. They also show broad wings of Hβ in absorption, the signature of early-type stellar photospheres. All of these feature are present in the nuclear spectra of SWB96 as well, although they classified it as a LINER. Although we have no optical spectra of our own to analyze, we favor slightly the interpretation of Véron et al. (1981) and García-Vargas et al. (1990), who concluded that the spectrum is a composite Seyfert 2/H II region. The LINER classification may simply be an artifact of applying line-ratio diagnostic diagrams to a two-component spectrum.
2. Kawara, Nishida & Gregory (1987) claimed to detect a broad Brackett γ line of atomic hydrogen from NGC 1672 with a width of $1\,100 \pm 380$ km s^{-1}. Their aperture size was 6×3.8 arcsec. In addition, they found that NGC 1672's K band and molecular hydrogen emission suggest that it has an active nucleus (see their sect. III.c). However, Moorwood & Oliva (1988) did not detect the Brackett γ line and set an upper limit on it that is a factor of about two below the detection of Kawara, Nishida & Gregory (1987). Their aperture size was 6×6 arcsec.
3. NGC 1672 has a compact radio source located at its optical nucleus (cf. Plate 2 of Harnett 1987). Lindblad & Jörsäter (1996) recently used the Australia Telescope National Facility to make synthesis maps of the nuclear region, and they find that it is composed of a small nucleus surrounded by an almost circular ring with a radius of about 5.4 arcsec (cf. SWB96; sect. 3 of Sandqvist, Jörsäter & Lindblad 1995). This ring is also seen in Hα, but the correlation between radio and Hα substructure is low. Tovmassian (1968) presented evidence that NGC 1672's 21 cm flux increased by at least a factor of 4 between 1962 and 1965 (there is no further data we know of which examines the claimed variability in more detail). The radio spectral index of Harnett (1987) is 0.73 ± 0.14, typical of optically thin synchrotron emission.

1.3 Previous X-ray observations

NGC 1672 was first detected as an X-ray source by the *Einstein* Observatory (Griffiths et al. 1979; Fabbiano, Feigelson & Zamorani 1982; Fabbiano, Kim & Trinchieri 1992). The 4.9 ks *Einstein* observation yielded 129 ± 16 counts after background subtraction. The X-ray emission was clearly extended but details of the shape were unclear. Crude spectral fitting to a power-law model was performed by Kruper, Urry & Canizares (1990). The observed 0.2–4.0 keV flux was $\approx 7 \times 10^{-13}$ erg cm^{-2} s^{-1}, corresponding to an isotropic luminosity of $\approx 6 \times 10^{40}$ erg s^{-1}.

The GINGA X-ray satellite made both scanning and pointed observations of NGC 1672 on 1991 Aug 3 with the Large Area Counter (LAC) instrument (Awaki & Koyama 1993). A hard X-ray source was seen during the scanning observations in the 0.3×4 degree error box. After background subtraction, the GINGA LAC count rate during the pointed observation was 2.1 count s^{-1} (the pointed observation had an entrance aperture of 1×2 degrees FWHM and no imaging capability within this aperture). The observed 2–10 keV flux was $\approx 3 \times 10^{-12}$ erg cm^{-2} s^{-1}, corresponding to a luminosity of $\approx 2 \times 10^{41}$ erg s^{-1}. The 2–10 keV photon index was measured to be 1.5 ± 0.2 (90 per cent confidence level errors), and the cold column was constrained to be less than 3×10^{22} cm^{-2}. We shall compare the GINGA and *ROSAT* data below.

2 OBSERVATIONS, DATA REDUCTION AND ANALYSIS

ROSAT PSPC (Trümper 1983; Pfeffermann et al. 1987) observations were made of NGC 1672 starting on 1992 Nov 29 (RP701021; total raw exposure of 20.0 ks). *ROSAT* HRI observations were made of NGC 1672 starting on 1992 Jun 24 (RH701022; total raw exposure of 24.4 ks). NGC 1672 was in the centres of the fields of view for both observations. The *ROSAT* observations were performed in the standard 'wobble' mode; to avoid accidental shadowing of sources by the coarse wire grid which forms part of the PSPC entrance window support structure, *ROSAT* performs a slow dithering motion diagonal to the detector axes with a period of ≈ 400 s and an amplitude of 3 arcmin.

Reduction and analysis of the PSPC and HRI data was performed with the Starlink ASTERIX X-ray data processing system.

2.1 Spatial analysis

2.1.1 X-ray sources and naming convention

Figure 1 shows contours of the adaptively smoothed HRI image overlaid on the image from the UK Schmidt

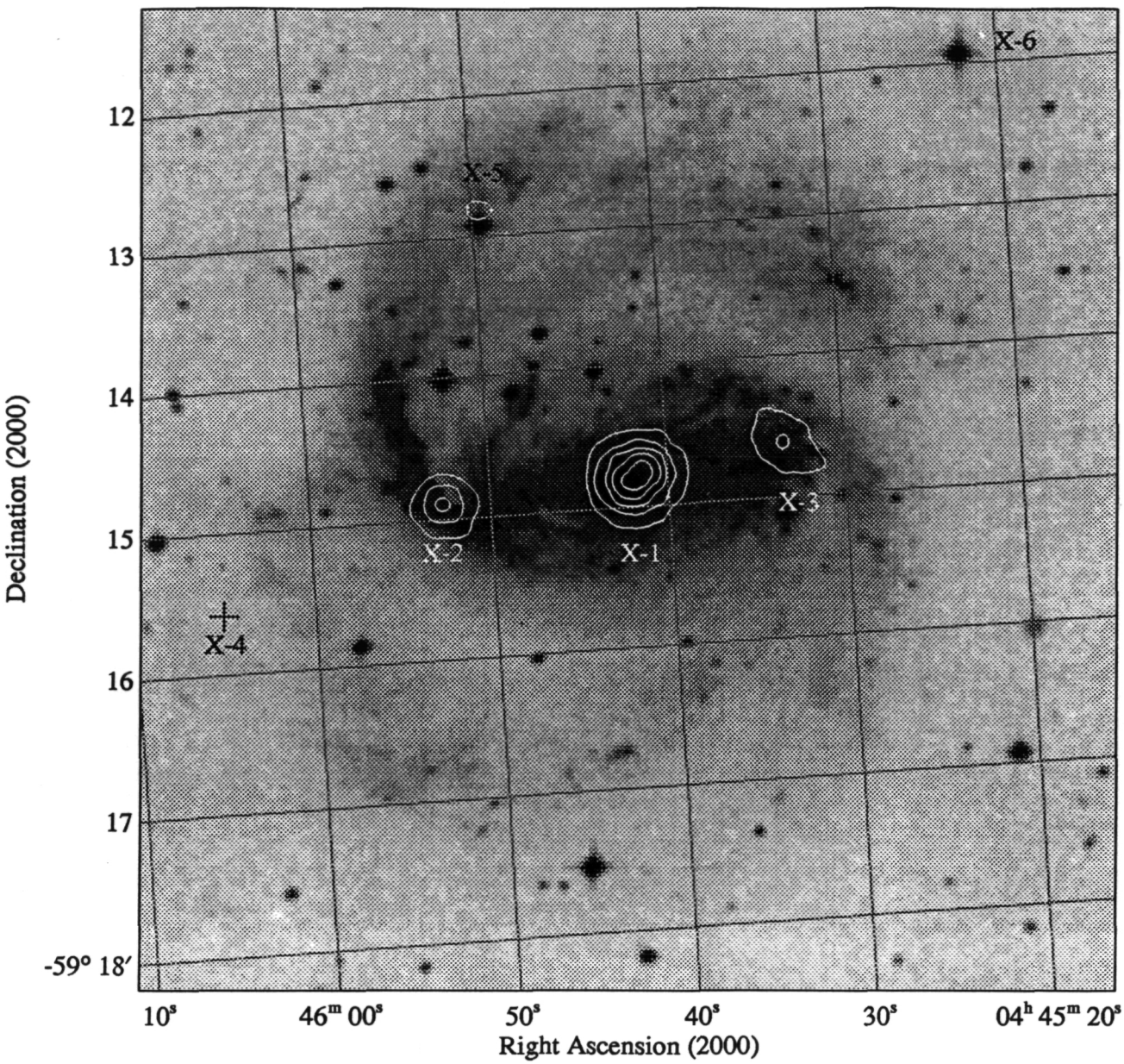

Figure 1. Contours of the adaptively smoothed HRI image overlaid on the image of NGC 1672 from the UK Schmidt southern sky survey J plate. Contours are at 6.4, 11.0, 19.2, 33.5 and 58.2 per cent of the maximum pixel value (see the text for absolute source fluxes). Note the strong central X-ray source and the location of X-ray sources at both end of the bar.

southern sky survey J plate (see sect. IIb of Lasker et al. 1990 for more information on the optical image). The adaptive smoothing algorithm is described in Rangarajan et al. (1995) and Ebeling & White, in preparation. We have set the area that we smooth over by requiring that 25 photons lie within it, and we use a circular tophat smoothing function. Figure 2 shows the adaptively smoothed PSPC image using PSPC channels 50–200. We have set the area that we smooth over by requiring that 10 photons lie within it. In Table 1 we list the positions of X-ray sources detected near NGC 1672 and give their statistical significances and numbers of counts.

NGC 1688 also lies in the field of view of the PSPC observation, but is not detected as an X-ray source. Starburst activity may not have been triggered in NGC 1688 by the putative interaction due to its smaller mass. The smaller galaxy is thought to be the gas loser in most interactions.

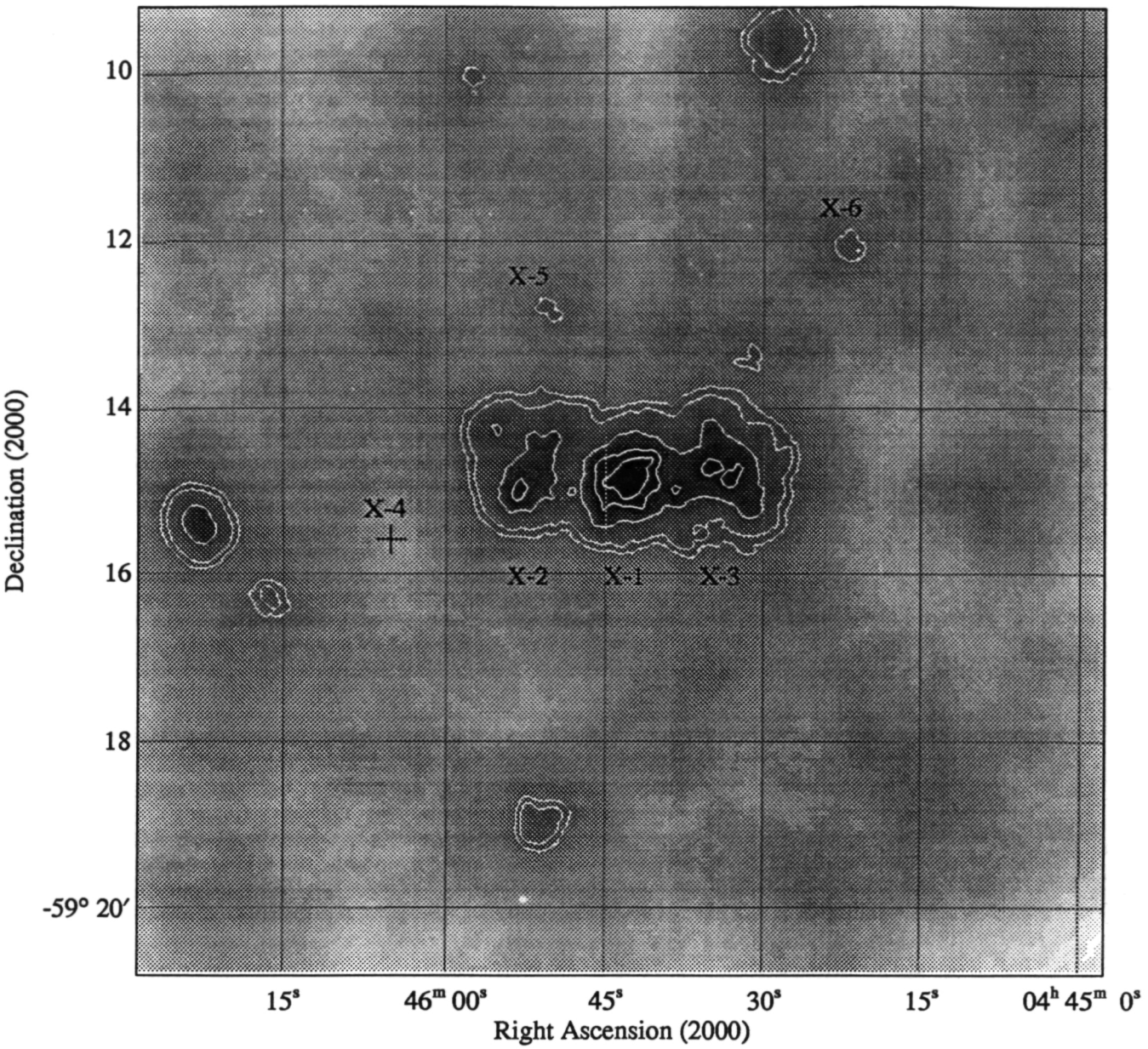

Figure 2. The adaptively smoothed PSPC image of NGC 1672 using PSPC channels 50–200. The shading is logarithmic and contours are at 1.1, 1.6, 5.1, 16.0 and 40.3 per cent of the maximum pixel value (see the text for absolute source fluxes).

2.1.2 Association of the X-ray sources with sources at other wavelengths

The compact radio core of NGC 1672 has a centroid position of α_{2000} = 04h45m42.48s, δ_{2000} = −59d14m50s (Lindblad & Jörsäter 1996), and this agrees with the X-ray centroid position of X-1 to within its error. The centroids of X-2 and X-3 are separated by 2.4 arcmin and lie at the ends of NGC 1672's bar. We also note that in the PSPC image there appears to be some weak emission from a separate pointlike source just to the Northwest of X-3. This emission coincides with an optically bright region along one of NGC 1672's arms (compare Figures 1 and 2).

X-4 is of interest because it lies reasonably close to NGC 1672's centre and because it is fairly firmly detected by the HRI yet not by the PSPC (despite the fact that the PSPC observation is deeper). The second fact suggests potential variability in this source. It lies about 0.5 arcmin off of the main part of one of the arms and there is no matching source on the UK Schmidt image or in NED.

X-5 is located near a bright foreground star which has an optical position of α_{2000} = 04h45m50s, δ_{2000} =

Table 1. X-ray sources near to NGC 1672.

Name	α_{2000}	δ_{2000}	Separation from X-1	HRI counts	HRI Sig.	PSPC counts	PSPC Sig.
	04 45 07.4	−59 20 17.1	7.0	8.0 ± 2.8	3.6	—	—
	04 45 08.2	−59 15 16.7	4.1	7.8 ± 2.8	3.4	5.6 ± 2.4	3.5
	04 45 11.4	−59 12 47.8	4.4	8.0 ± 2.8	3.7	—	—
X-6	04 45 21.7	−59 12 00.0	4.0	14.1 ± 3.8	4.1	7.7 ± 2.7	4.5
	04 45 28.8	−59 09 27.3	5.7	14.0 ± 3.7	4.1	29.5 ± 5.4	8.3
X-3	04 45 33.9	−59 14 40.3	1.1	73.3 ± 8.6	8.0	179.8 ± 13.4	25.1
	04 45 40.6	−59 17 47.9	2.9	7.5 ± 2.7	3.1	5.2 ± 2.3	3.6
X-1	04 45 42.2	−59 14 51.1	0.0	217.5 ± 14.7	26.4	452.5 ± 21.3	51.8
X-5	04 45 49.8	−59 12 48.9	2.3	15.5 ± 3.9	5.4	9.3 ± 3.1	4.1
	04 45 51.2	−59 18 59.9	4.3	—	—	12.1 ± 3.5	5.8
	04 45 51.1	−59 10 52.0	4.0	7.0 ± 2.6	2.9	6.2 ± 2.5	3.2
X-2	04 45 53.2	−59 14 57.8	1.4	62.0 ± 7.9	10.6	117.1 ± 10.8	19.4
	04 45 58.8	−59 10 15.0	5.1	—	—	7.9 ± 2.8	4.0
X-4	04 46 05.1	−59 15 34.8	3.0	12.0 ± 3.4	4.3	—	—
	04 46 16.5	−59 16 14.7	4.6	—	—	15.8 ± 4.0	5.3
	04 46 23.2	−59 15 26.8	5.2	15.0 ± 3.9	5.3	33.3 ± 5.8	11.7

α_{2000} and δ_{2000} give the J2000 X-ray centroid positions as determined with the ASTERIX program PSS. We quote HRI positions whenever possible but when sources are only detected by the PSPC we quote PSPC positions. HRI positions have errors of ≈ 5 arcsec and PSPC positions have errors of ≈ 20 arcsec taking into account boresight and other positional errors. The third column is the separation in arcmin between the centroid of the source and the centroid of source X-1 (which lies in the centre of NGC 1672). HRI counts and PSPC counts are the raw number of counts after background subtraction. When determining the number of counts we use the full HRI band and channels 50–200 (corresponding to 0.5–2.0 keV) of the PSPC band. HRI and PSPC significances are determined using PSS. When determining significances we use the full HRI band and channels 50–200 of the PSPC band. We list all sources that are detected with greater than 3.5σ significance by either the HRI or the PSPC (and we list the significance of the source in the complementary detector as well if this significance is greater than 2.8 sigma).

−59d12m56s. The separation between the optical star and the X-ray centroid is 7 arcsec, and this is the most probable identification for the X-ray source. The star is not listed in SIMBAD and we have not been able to correct its optical position for any proper motion. Similarly, X-6 also appears to be associated with a foreground star.

The other unnamed sources listed in Table 1 do not have any bright optical counterparts. Many of them are probably background sources.

2.1.3 X-ray spatial extents

In Figure 3 we plot HRI radial brightness profiles of X-1, X-2 and X-3. In making this figure, we have conservatively excluded HRI channels 1–3 to avoid any contamination by UV light (cf. sect 3.6 of David et al. 1995). Source X-1 and perhaps source X-3 appear to be extended when compared to the HRI point spread function (PSF; we obtain the PSF from Section 3.2.3 of David et al. 1995 and consider the empirical range of PSFs discussed there). We are aware of the effects the wobble can have on source extensions (cf. Morse 1994), but we are in the fortunate position of having three sources to compare. The fact that X-1 is significantly more extended than X-2 strongly suggests that its apparent extent is real and not an artifact of the wobble. Similarly, the extent of X-3 is also probably real. None of the sources in the HRI field are bright enough to allow us to perform wobble correction using the Morse code HRIASPCOR in FTOOLS.

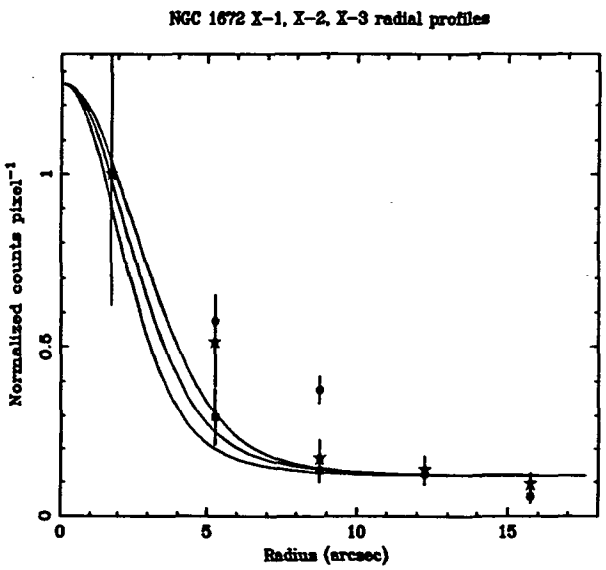

Figure 3. HRI radial profiles of NGC 1672 X-1 (circles), X-2 (squares) and X-3 (stars). Each source's first data point is normalized to unity. The expected range of the HRI PSF from David et al. (1995) is graphed as the three solid curves, shifted so that they asymptotically match the background level.

2.1.4 *Source count extractions for light curves and spectra*

When preparing the light curves and spectra presented below, we have extracted the source counts from carefully chosen source cells that include as many source counts as possible while minimizing cross-source contamination at low energies between X-1, X-2 and X-3. This is difficult in the regions between the sources due to the electronic 'ghost imaging' which widens the point spread function below about 0.3 keV (Hasinger et al. 1992). We discuss this issue in more detail below.

Background counts were subtracted from the source cells using large, nearby circular source-free background cells. Corrections were included for detector dead time, vignetting and shadowing by the coarse mesh window support.

2.2 Temporal analysis

Count rates should be averaged over an integer multiple of the 400 s *ROSAT* wobble period when used for source flux determination (cf. Brinkmann et al. 1994). We do not detect any highly statistically significant variability of X-1, X-2 or X-3 within either the PSPC or the HRI data. When we compare count rates for X-1, X-2 and X-3 using the PIMMS software and the best fitting spectral models described below, there is no strong evidence for variability between the PSPC and HRI observations.

2.3 Spectral analysis

2.3.1 *Relative X-ray energy distributions*

To gain model independent insight into the spectral differences between X-1, X-2 and X-3, we compared their relative X-ray spectral energy distributions (Figure 4). Counts from the corrected PSPC source cells were binned so that one data point in Figure 4 corresponds to 30 PSPC channels, and we have ignored channels below 30 to minimize cross-source contamination. Note that X-1 is the softest of the three sources while X-3 is the hardest.

2.3.2 *Binning and calibration of source spectra*

For our spectral fitting, counts from the corrected PSPC source cells were binned into 256-channel, pulse-invariant spectra. We ignored channels 1–8 and rebinned the extracted spectra so that at least 20 source photons were present in each bin.

Systematic errors of 2 per cent were added in quadrature to the data point rms errors to account for residual uncertainties in the spectral calibration of the PSPC. We have used the 1993 January response matrix. It corrects for the systematic deficit of photons near the carbon edge of the PSPC detector that was present in earlier matrices (cf. Turner, George & Mushotzky 1993). The expected systematic errors from this matrix are a few per cent.

2.3.3 *Spectral fitting preliminaries and information about neutral hydrogen column*

We model the X-ray spectra presented below using the spectral models in the XSPEC fitting package (Shafer et al. 1991).

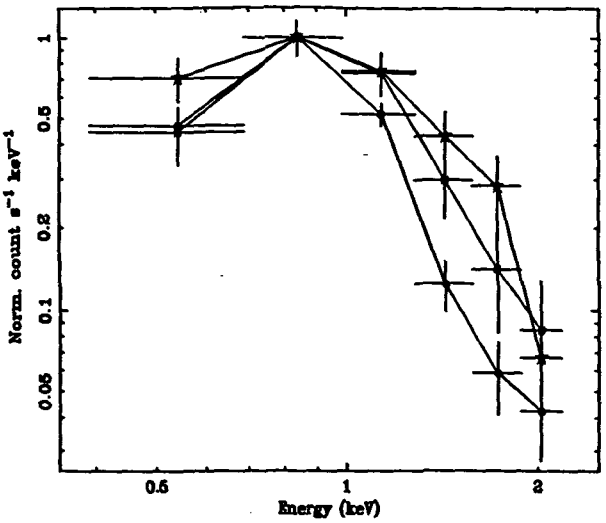

Figure 4. PSPC spectra of NGC 1672 X-1 (circles), X-2 (squares) and X-3 (stars). These spectra have been normalized so that their maxima correspond to unity. Note the relative numbers of hard counts from each source.

The errors for all fits shall be quoted for 90 per cent confidence (unless explicitly stated otherwise), taking all free parameters to be of interest other than absolute normalization (Lampton, Margon & Bowyer 1976; Press et al. 1989).

Due to the southerly declination of NGC 1672, its Galactic neutral hydrogen column density is not given in any of the 21 cm catalogs. Fabbiano et al. (1989) adopted a Galactic column of $N_{\rm H} = 3.0 \times 10^{20}$ cm^{-2} to NGC 1672 because of its high Galactic latitute ($-39°$).

The nuclear region of NGC 1672 has a large Balmer decrement of $H\alpha/H\beta \approx 10$, which OSW74 argue is caused by dust reddening in NGC 1672 with $E(B-V) \approx 1.3$. If we assume a 'Galactic' dust-to-cold-gas ratio, the corresponding neutral hydrogen column density is $N_{\rm H} \approx 7 \times 10^{21}$ cm^{-2} (cf. sect. VI of Burstein & Heiles 1978). However, SWB96 argue that the Balmer emission lines need to be corrected for the underlying absorption lines of the early stellar population, which affects $H\beta$ more strongly than $H\alpha$. After subtracting an appropriate stellar template spectrum, the resulting Balmer decrement at the nucleus corresponds to $E(B-V) \approx 0.16$, or $N_{\rm H} \approx 9 \times 10^{20}$ cm^{-2}. However, $E(B-V)$ values of 0.4–0.6 are seen within the spatial region corresponding to X-1. Interestingly, the derived extinction is smaller in the nucleus than in regions of surrounding star formation, in which $E(B-V)$ as large as 0.7 is seen (see Table 9 of SWB96).

Despite its large Balmer decrement and significantly reddened UV continuum, the *IUE* spectrum of NGC 1672 (Kinney et al. 1993) shows no evidence of the 2175 Å dust absorption feature often associated with small graphite grains (e.g. sect. 1.4 of Tielens & Allamandola 1987; sect. 2.1.2 of Mathis 1990). This peculiar effect has been seen in many star forming galaxies (sect. 4.2.4 of Kinney et al. 1993; Calzetti, Kinney & Storchi-Bergmann 1994). It may suggest either an unusual dust chemical composition/grain size distribution or clumpy dust that acts as a 'picket fence' (we discuss and examine these possibilities below). The

weakness of the 2175 Å feature in parts of the LMC and SMC is often attributed to their low metallicities (e.g. sect. 45.5 of Lequeux 1988). There is also evidence that the carriers of the 2175 Å feature are very sensitive to the strength of the local radiation field (Leene & Cox 1987; Rosa & Benvenuti 1995). The depth of the absorption feature decreases as the radiation field gets stronger, perhaps due to the destruction of the carrier particles.

In the following sections, we shall refer to dust that lacks the carrier of the 2175 Å feature (either due to a peculiar chemical composition or grain size distribution) as CDD ('carrier deficient dust').

2.3.4 Spectral fitting to NGC 1672 X-1

The *ROSAT* PSPC spectrum of X-1 is shown in Figure 5. To avoid confusion by cross-source contamination, we fit only the data above PSPC channel 30 where X-1, X-2 and X-3 are fairly cleanly separated. A power-law model, as might be expected if electron scattered X-ray emission from a Seyfert nucleus dominated the spectrum, is statistically unacceptable ($\chi^2_\nu = 2.0$) and gives an unphysically steep photon index ($\Gamma > 10$). This is understandable due to the very steep drop-off in X-ray flux above ≈ 1 keV. If we fit only the data above PSPC channel 50, a simple power-law model can still be ruled out with greater than 95 per cent confidence unless its photon index is greater than 6.0. Such a steep soft X-ray spectrum is never seen Seyfert galaxies and thus a simple power-law model for X-1 is unphysical. The residuals suggest that a power-law fit is poor due to the robust overall shape of the spectrum and not due to just a few stray data points. Deleting sets of points confirms this conclusion.

Electron scattering mirrors in which the atoms in the mirror are not fully stripped of their electrons can also imprint X-ray emission lines on a scattered X-ray spectrum. The strongest such emission lines in the *ROSAT* band are from iron L. We consider an electron scattering mirror that imprints iron L lines by fitting our data to an absorbed power-law model with a Gaussian emission line. The centroid energy of the line is chosen to lie in the range 0.85–1.0 keV, and the line width (σ) is chosen to lie in the range 0.05–0.20 keV (this is a reasonable model for the iron L complex given the limited spectral resolution of *ROSAT* and the small number of counts in our spectrum). While some choices of line parameters in these ranges give statistically acceptable fits, the underlying photon indices derived from such fits are always significantly larger (> 2.5) than are seen in Seyfert 2 galaxies (the soft X-ray spectra of Seyfert 2's are flattened in scattering and have photon indices in the range 1.0–1.6). In addition, the iron L complex equivalent widths derived from our fitting are always larger than 700 eV (and flatter spectra tend to require larger iron L complex equivalent widths). Such equivalent widths, while not impossible, are large compared to what is seen in, for example, Mrk 3 (Iwasawa et al. 1994).

Simple absorbed bremsstrahlung and blackbody models are poor fits to the data and can be rejected with > 99 and > 95 per cent confidence, respectively. They both leave large systematic residuals in the 0.7–1.0 keV range.

Massive or low-mass X-ray binary sources similar to those in the Milky Way are not likely to make major contributions to X-1's *ROSAT* band X-ray flux due to its soft spectrum and fairly steep X-ray drop-off above ≈ 1 keV (cf. sect. III.b of Fabbiano 1988; sect. 4.2 of David, Jones & Forman 1992). They may, of course, contribute significantly at higher energies. Some contribution from 'supersoft' X-ray binaries to the *ROSAT* flux may be possible.

A Raymond-Smith thermal plasma model with cold absorption gives a good fit with $N_{\rm H} = (1.6^{+2.4}_{-1.6}) \times 10^{20}$ cm^{-2}, $kT = 0.68^{+0.15}_{-0.08}$ keV and $\chi^2_\nu = 0.7$. The quality of the thermal plasma fit, the arguments above regarding scattered X-ray emission, and the significant spatial extent of X-1 suggest that the starburst activity in NGC 1672 dominates its X-ray emission along our line of sight (although we cannot rigorously rule out a substantial contribution of scattered X-rays from a Seyfert nucleus). The derived metal abundance by number relative to the cosmic one (Anders & Grevesse 1989) is $0.12^{+0.40}_{-0.08}$. Such a low derived abundance in the centre of a spiral galaxy appears surprising, and such a low abundance is not suggested by observations at other wavelengths (e.g. Alloin et al. 1979; Storchi-Bergmann, Calzetti & Kinney 1994; SWB96). It must be remembered, however, that due to our limited number of counts we only fitted a single temperature plasma model to what is probably emission from a multiple temperature plasma. This simplification can confuse abundance determinations. Fits with two solar-abundance Raymond-Smith plasmas are statistically acceptable and physically reasonable, albeit poorly constrained by our data. In addition, scattered X-rays from the Seyfert nucleus could further complicate the spectrum (although as explained above we suspect they do not dominate it). Fluxes and the isotropic luminosity of X-1 are given in Table 2.

The fitted cold hydrogen column is consistent with what we expect for the Galactic column, and we do not see evidence for absorption by gas associated with the large amounts of dust discussed by OSW74. This remains true even if we fix the abundance at the cosmic one (or several times it). Multi-component models, which include an additional thermal plasma or power-law component, do not facilitate the presence of a neutral column as large as would be expected based on OSW74. If we fix the column at $N_{\rm H} = 7 \times 10^{21}$ cm^{-2} (see the previous section for why we choose this value), we are not able to obtain statistically acceptable fits even with complicated spectral models (the fits are always poor below 0.5 keV). The same is true even if we lower the column to $N_{\rm H} = 3 \times 10^{21}$ cm^{-2}. A column of $N_{\rm H} = 9 \times 10^{20}$ cm^{-2} (again see the previous section) can be statistically accomodated by multi-component model fits, although the best fitting multi-component models generally have columns of $< 5 \times 10^{20}$ cm^{-2}. We shall discuss the absorption of the nuclear source in more detail below.

If we include the data points below 0.3 keV in our fitting, our results are not significantly changed from those above.

2.3.5 Spectral fitting to NGC 1672 X-2 and X-3

We shall again use only the data above PSPC channel 30 to prevent cross-source contamination. Due to the small numbers of counts from X-2 and X-3, our spectral models are not tightly constrained, and we shall quote 68.3 per cent confidence errors throughout this section.

A simple absorbed power-law model for X-2's spec-

Table 2. Raymond-Smith thermal plasma models of X-ray sources in NGC 1672.

Quantity	Source X-1	Source X-2	Source X-3
χ^2_ν	0.7	0.7	0.6
kT (keV)	$0.68^{+0.15}_{-0.08}$	$1.1^{+1.2}_{-0.3}$	$1.7^{+1.3}_{-0.6}$
Abundance ⋆	$0.12^{+0.40}_{-0.08}$	< 0.26	< 0.38
$N_{\rm H}/(1 \times 10^{20}$ cm$^{-2})$	$1.6^{+2.4}_{-1.6}$	3.0†	3.0†
(0.1–2.5 keV Absorbed $F_{\rm X}$)$/(1 \times 10^{-13}$ erg cm^{-2} s^{-1})	2.6	0.87	1.1
(0.1–2.5 keV Unabsorbed $F_{\rm X}$)$/(1 \times 10^{-13}$ erg cm^{-2} s^{-1})	3.6	1.3	1.5
(0.1–2.5 keV $L_{\rm X}$)$/(1 \times 10^{40}$ erg s^{-1})	2.1	0.76	0.88
$EM/(1 \times 10^{63}$ cm$^{-3})$	2.2	1.2	1.0
n (cm^{-3})	> 0.17	> 0.36	> 0.17
M (M$_\odot$)	$< 1.1 \times 10^7$	$< 2.8 \times 10^6$	$< 4.8 \times 10^6$
E (erg)	$< 1.4 \times 10^{55}$	$< 5.8 \times 10^{54}$	$< 1.6 \times 10^{55}$
P (dyne cm^{-2})	$> 3.8 \times 10^{-10}$	$> 1.3 \times 10^{-9}$	$> 9.6 \times 10^{-10}$

We quote 90 per cent errors for X-1 and 68 per cent errors for X-2 and X-3. EM is the emission measure, calculated as is described in the 'Raymond' model description of Shafer et al. (1991). n is the mean emitting gas density averaged over the source, M is the mass of the emitting gas, E is the thermal energy content of the emitting gas and P is the pressure of the emitting gas. Our calculations of n, M, E and P parallel those given in sect. 4.1 of Armus et al. (1995), and we have assumed homogeneous spherical emission regions. We take the radial extent of X-1 to be less than 8 arcsec, which corresponds to 880 pc; the radial extent of X-2 to be less than 4 arcsec, which corresponds to 440 pc; and the radial extent of X-3 to be less than 6 arcsec, which corresponds to 660 pc (see Figure 3).

⋆ Note that the ROSAT fit abundances are probably not physically meaningful; see the text.

† Column fixed at this value (see the text).

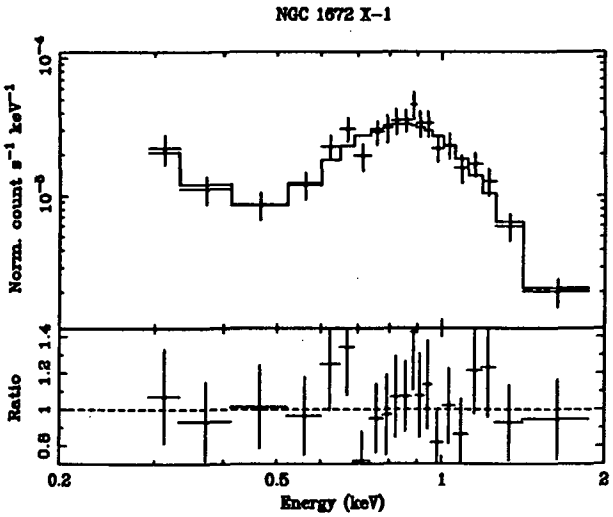

Figure 5. PSPC spectrum of NGC 1672 X-1. A Raymond-Smith thermal plasma model with cold absorption is also shown with the corresponding data-to-model ratio.

trum gives $\Gamma = 2.6^{+2.0}_{-0.8}$, is consistent with the Galactic column, and cannot be ruled out on statistical grounds (it has $\chi^2_\nu = 0.7$). However, given the starburst nature of X-2's location, we suspect that an absorbed Raymond-Smith thermal plasma model may be more appropriate. Using this model we obtain $N_{\rm H} = (3.9^{+24}_{-3.9}) \times 10^{20}$ cm^{-2}, $kT = 1.0^{+5.1}_{-0.7}$ keV and $\chi^2_\nu = 0.9$ (the associated abundance is not well constrained). In the above fitting the parameters are loosely constrained due to the fact that the neutral hydrogen column can become very high. If we assume there is no significant intrinsic hydrogen column and fix the column at $N_{\rm H} = 3.0 \times 10^{20}$ cm^{-2} (this is at least plausible for NGC 1672's inclination and our results for X-1), we obtain $kT = 1.1^{+1.2}_{-0.3}$ keV and $\chi^2_\nu = 0.7$. The associated abundance is constrained to be less than 26 per cent of the cosmic value (but see the important caveats in the previous section). Fluxes and the isotropic luminosity of X-2 may be found in Table 2.

A simple absorbed power-law model for X-3's spectrum gives $\Gamma = 2.0^{+1.2}_{-0.7}$, is consistent with the Galactic column, and cannot be ruled out on statistical grounds (it has $\chi^2_\nu = 0.6$). As per X-2, however, we suspect that an absorbed Raymond-Smith thermal plasma model may be more appropriate. Using this model we obtain $N_{\rm H} = (2.5^{+11}_{-2.5}) \times 10^{20}$ cm^{-2}, $kT = 1.8^{+5.0}_{-0.8}$ keV and $\chi^2_\nu = 0.7$ (the associated abundance is not well constrained). If, as per the previous paragraph, we fix the column at $N_{\rm H} = 3.0 \times 10^{20}$ cm^{-2}, we obtain $kT = 1.7^{+1.3}_{-0.6}$ keV and $\chi^2_\nu = 0.6$. The associated abundance in constrained to be less than 38 per cent of the cosmic value. Fluxes and the isotropic luminosity of X-3 may be found in Table 2.

2.3.6 Comparison of ROSAT and GINGA spectral results

Using the GINGA spectral parameters given in Sect. 1 and the *ROSAT* spectral parameters and data described above, we have compared the spectra from these two satellites. If the GINGA spectral data were dominated by a central active nucleus in NGC 1672 and the flux from this nucleus did not vary with time, then one would expect the low-energy end of the GINGA spectral model to join fairly smoothly

onto the high-energy end of the *ROSAT* PSPC X-1 spectrum. This is not observed. Instead the low-energy end of the GINGA spectral model is a factor of ≈ 7 times higher than the high-energy end of the *ROSAT* PSPC spectrum of X-1, even when the upper limit on the column given by Awaki & Koyama (1993) is used. This suggests that either the GINGA spectral data were not dominated by a central active nucleus in NGC 1672 (at least at the low-energy end of the GINGA band) or the hard X-ray flux from the central nucleus decreased between the GINGA (1991 Aug 3) and *ROSAT* (1992 Nov 29) observations. We cannot rule out hard X-ray variability, and such variability may be probed for with future observations. Obvious additional contributors to the GINGA spectrum could be X-ray binaries in X-2 and X-3. If we create a *ROSAT* spectrum that includes all the emission from X-1, X-2 and X-3, then the agreement between the GINGA and *ROSAT* data is significantly improved (even though X-2 and X-3 are weaker overall than X-1, note from Fig. 4 that they are harder). The mismatch between the low-energy end of the GINGA spectral model and the high-energy end of the *ROSAT* data is only a factor of ≈ 2. If, as our analysis suggests, X-2 and X-3 contribute to the GINGA flux, then the true column density to the nuclear source is probably larger than the upper limit that GINGA measured. Of course, sources external to NGC 1672 could also contribute to the GINGA flux. Our *ROSAT* field does not have any sources that are much stronger than NGC 1672 in it, but there are four sources of roughly comparable soft X-ray flux that could contribute hard flux.

3 DISCUSSION

3.1 Source X-1

3.1.1 Optical, UV and X-ray absorption

Our *ROSAT* spectrum constrains the *flux-weighted* average amount of neutral gas (both in atomic and molecular form) along our lines of sight to the X-ray sources in the nuclear region. The fact that we do not see a large cold column associated with the nuclear region (from our fitting to X-1), combined with its other absorption properties (optical reddening, UV continuum reddening, lack of 2175 Å feature; see sect. 2.3.3), suggests either peculiar absorption physics or an interesting source geometry. We shall adopt the optical reddening analysis of TWB96 rather than that of OSW74.

In this paragraph we examine how/whether peculiar absorption physics might explain the optical, UV and X-ray absorption properties. We shall make the assumption that the optical, UV and X-ray emissions all traverse a screen of matter between their sources and Earth (we shall then examine the case when this assumption is false). Cold gas associated with the CDD described Sect 2.3.3 might explain the X-ray data if the X-ray spectrum has multiple components. A somewhat larger than 'Galactic' dust-to-cold-gas ratio is suggested, however. If the some of the gas associated with the dust were ionized (so that it did not contribute to the cold X-ray column), this could explain the higher suggested value of this ratio. Another possible type of screen that could be traversed by the optical, UV and X-ray emissions on their way to Earth is one that consists of thick clumps of dust along the line of sight ('picket fence' dust as discussed in sect. 4.2.4 of Kinney et al. 1993; hereafter PFD). PFD might explain the lack of the 2175 Å feature if the dust clumps were opaque to the UV and thus just lowered the detected UV flux without changing the UV spectral shape (i.e. imprinting the 2175 Å feature). However, such clumps then have difficulty explaining the large Balmer decrement and the reddened UV continuum. Thus a PFD model for the nuclear region's absorption seems to be untenable.

Now we examine how/whether source geometry might explain the optical, UV and X-ray absorption properties. We shall not make the assumption that the optical, UV and X-ray emissions all traverse an absorbing screen between their sources and Earth. Because the X-ray fits to X-1 provide a *flux-weighted* average measure of the amount of neutral gas between us and the X-ray sources in the nuclear region, heavily absorbed sources that are faint as a result of absorption by neutral gas will contribute less to this average than similar sources that are not heavily absorbed (cf. sect. 1 of Witt, Thronson & Capuano 1992). Thus, the true average amount of absorbing gas present might be underestimated by the fitted cold X-ray column. Similar considerations apply to the optical and UV emissions. In light of this argument, a model to explain the absorption properties of the nuclear region might involve some sources that are heavily obscured and some that are not (along the lines of what is discussed in sect. 3.6 of Calzetti, Kinney & Storchi-Bergmann 1994). The heavily obscured sources would produce the large observed *nebular* Balmer decrement, while the sources that are not heavily obscured would not contribute significantly to the Balmer lines since they lack the requisite nebulae. The sources that are not heavily obscured would dominate the optical continuum, the ultraviolet continuum longward of 1200 Å (hence diluting away any 2175 Å feature), and the soft X-ray continuum (hence leading to the low $N_{\rm H}$ fit value).

Another geometrical way to explain the optical, UV and X-ray absorption properties would be to locate the optical and UV sources behind a CDD screen as above, but not the X-ray emitting sources. Such a situation might be realized if X-ray emitting gas were expelled to a position outside or above the screen, perhaps by a superbubble or superwind. A point in favour of this general idea is the erratic behaviour of the [O III] lines near the nucleus. As noted by Lindblad & Jörsäter (1996), large velocity jumps and changes of shape occur over distances of an arcsec. These authors speculate that this behaviour is due to an outflow directed close to the line of sight. This is in line with what might be expected for a starburst superwind, and if a superwind deposited gas above the plane of NGC 1672 this could explain the small X-ray column that we measure. The spatial extents of X-1 and X-3 appear to be larger than the ~ 150 pc scale height of a typical galactic interstellar medium, and this fact also suggests that a significant amount of X-ray emitting gas may lie above the starburst region (which is probably confined to about the height of the molecular cloud layer).

3.1.2 Comparison with other wavelengths and the origin of the soft X-ray emission

The soft X-ray isotropic luminosity we derive for X-1 is only a small fraction of the total isotropic luminosity of NGC 1672's central region. In the near-infrared the K-band nu-

clear isotropic luminosity in a 3 arcsec diameter aperture is 1.0×10^{42} erg s^{-1} (Forbes et al. 1992), and significant extended emission is seen as well. In the far-infrared, NGC 1672 has a 40–120 μm isotropic luminosity of 9.6×10^{43} erg s^{-1} (Maia et al. 1994 corrected to $H_0 = 50$ km s^{-1} Mpc^{-1}).

The 5000 MHz (6 cm) radio luminosity of NGC 1672 is 3.2×10^{38} erg s^{-1}. Comparison of our spatially resolved X-ray maps and Plate 2 of Harnett (1987) is revealing. It shows that despite the fact that X-1 is only stronger than X-2 or X-3 by a factor of ≈ 2.5, the central region is at least 15 times more powerful than the regions near X-2 and X-3 at 843 MHz (36 cm). The fact that the central region is $\gtrsim 6$ times more efficient at producing 843 MHz radio flux per unit X-ray flux immediately suggests that either (1) the energy generation mechanism in the central region is different from those near X-2 and X-3 or (2) there is an additional producer of radio flux associated with the central region that does not generate large amounts of X-ray flux. Although our constraints on the best-fit X-ray specta of X-2 and X-3 are not tight, their spectra do not appear to be strongly different from that of X-1 (although they are somewhat harder), suggesting that the X-ray generation mechanisms may not be strongly dissimilar. The spectral luminosity of NGC 1672 at 1410 MHz (21 cm) is 2.4×10^{22} W Hz^{-1}. Comparison with fig. 4 of Ulvestad & Wilson (1984) shows that this is a fairly typical 1410 MHz spectral luminosity for a Seyfert nucleus, although comparison with fig. 1 of Davies (1989) shows that it is not entirely out of the range of 'normal' spirals.

Using a 20 arcsec aperture, OSW74 measured an uncorrected Hβ isotropic luminosity from NGC 1672 of 1.6×10^{40} erg s^{-1} (we correct to the distance of Sect. 1.1). After correcting for their $E(B-V) = 1.3$, they infer a true Hβ isotropic luminosity of 1.1×10^{42} erg s^{-1}. They also pointed out that the appropriate correction could be even larger than this if internal dust is present. However, if we adopt a smaller average $E(B-V)$ of $\simeq 0.5$ from the starlight-subtracted, near-nuclear measurements of SWB96, then the intrinsic Hβ luminosity is only increased to 8×10^{40} erg s^{-1}. The true value is perhaps somewhere between these extremes. The Lyman continuum photon number derived by OSW74 from their corrected Hβ isotropic luminosity is 1.7×10^{54} photons s^{-1}. Ward (1988) used the Brackett γ data of Kawara, Nishida & Gregory (1987) to derive an ionizing photon number of 1.1×10^{53} photons s^{-1} (we correct to the distance of Sect. 1.1). The latter estimate is much less dependent on the correction for dust absorption than the estimate of OSW74 (although none has been made), and is derived using a smaller aperture size of 6×3.8 arcsec. Given the size of the nuclear region in NGC 1672, the discrepancy of a factor of ≈ 9 between these two measurements might be partly due to the different aperture sizes. In addition, however, it probably supports the lower extinction estimates of SWB96. Thus the calculation of Ward (1988) is in general agreement with Balmer-line measurements in the nuclear region of NGC 1672, although the data of Moorwood & Oliva (1988) show that any conclusions drawn from the Brackett γ data on NGC 1672 of Kawara, Nishida & Gregory (1987) must be treated with caution. Based on their Lyman photon counting, OSW74 suggested that about 160 000 ionizing stars are present in the nuclear region, together with the rest of a young stellar population. The extinction values of SWB96, on the other hand, argue that the true number is probably a factor of about 10 smaller.

The Lyman continuum photon number of Ward (1988) is ~ 11 times larger than that from the R136 nebula of 30 Doradus ($\gtrsim 10^{52}$ photons s^{-1}; Wang & Helfand 1991), the most luminous H II region in the Local Group. If we assume identical stellar-type distribution functions for the central region of NGC 1672 and the R136 nebula, the number of ionizing stars in the central region of NGC 1672 will be ~ 11 times larger than that in the R136 nebula. If we scale the soft X-ray luminosity of the R136 nebula ($(1\text{–}4)\times 10^{37}$ erg s^{-1}; Wang & Helfand 1991) by this factor, we derive a characteristic soft X-ray luminosity of only $(1\text{–}4.4)\times 10^{38}$ erg s^{-1}. This is to be compared with X-1's isotropic luminosity in soft X-rays of 2×10^{40} erg s^{-1}. Even if we adopt the larger Lyman continuum flux of OSW74, we can only account for $(2\text{–}7)\times 10^{39}$ erg s^{-1} by analogy with R136. Hence the nuclear activity in the central region appears to be more efficient in generating X-rays per Lyman continuum photon than the activity in R136, perhaps due to a larger fractional contribution from non-stellar processes such as supernovae, or heating by a hidden Seyfert 1 nucleus.

It is unlikely that O stars directly produce most of X-1's X-rays. For a typical O star luminosity of 5×10^{33} erg s^{-1} (cf. Harnden et al. 1979), about four million O stars would be required. However, most of the X-rays associated with O stars do not come directly from the stars themselves but instead from the energy that their winds and supernovae deposit in the interstellar medium. Following the argumentation in sect. 3.2 of Wang & Helfand (1991) and taking into account the ≈ 8 Myr age (Díaz 1985), it is energetically possible that X-1 arises from a violent interstellar medium similar to that seen in R136 but on a much larger scale. Stellar winds carve out hot cavities in the neutral interstellar medium and subsequent supernovae occur in hot, low-density environments where they do not form bright remnants but do heat the hot component of the interstellar medium. Our X-ray spectral fitting results are in reasonable agreement with this interpretation. The Raymond-Smith temperature of $7.0\text{–}9.6\times 10^6$ K is not dissimilar to the $\approx 6 \times 10^6$ K Raymond-Smith temperature of R136. We have considered contributions to the soft X-ray spectrum from X-ray binaries in Sect. 2.3.4.

In Table 2 we present emission measures for our thermal plasma fits as well as quantities we estimate from these emission measures. The thermal plasma models for X-1, X-2 and X-3 imply surprisingly large densities and thermal energy contents. Because the apparent radius of each source is relatively small, we are forced to consider particle densities of order 0.2 and larger. X-1, X-2 and X-3 contain energies corresponding to about 10^3–10^4 supernovae. Although the sizes and temperatures of these regions are comparable to those expected for superbubbles blown by this many supernovae over a 10^7 yr period (MacLow & McCray 1988, hereafter MM88), their inferred internal densities are much greater, even when the evaporation of the cold dense shell to the interior is included (see eqn. 5 of MM88). The internal pressure of X-1 corresponds to 140 times that of the nearby hot ISM (Bowyer et al. 1995; note that X-2 and X-3 have even higher pressures than X-1). The ambient density required by eqn. 5 of MM88 is ~ 300 cm^{-3}, much higher than the average value that would be expected over an extent of > 440 pc in a spiral galaxy. The amount of mass swept out

of X-1 would be $\sim 10^{10}$ $M_\odot$, an implausible amount. Another argument against such large ambient densities is the absence of X-ray absorption by the correspondingly dense HI supershells which would surround the superbubbles.

What aspect of this scenario could be altered to retain a plausible thermal plasma model? First, the derived emission measures might be overestimates if the fitted abundances are in error. It is difficult, if not impossible, to measure abundances reliably using *ROSAT* data. If the actual metal abundances were the solar ones, for example, then we estimate with XSPEC that the derived emission measure of X-1 could be lower by a factor of about 6. The same argument applies to X-2 and X-3. Indeed, SWB96 derived abundances that are slightly higher than solar in the nuclear region of NGC 1672, and approximately solar along the bar. However, since the average number density only scales as the square root of the emission measure it is hard to imagine that the density could be reduced by more than a factor of four with such a correction. Second, if the hot medium were clumped as a result of the supernova explosions taking place among a large number of giant molecular clouds which have been completely shocked, but have not finished expanding, then the required mass and energy content would be reduced since they scale as the filling factor to the one half power (see sect. 4.1 of Armus et al. 1995; the filling factor is less than unity). Together, these two effects may render plausible a model in which one or more of the main X-ray sources in NGC 1672 are extremely luminous examples of superbubbles of the type envisioned by MM88, and thought to be seen by *ROSAT* in NGC 5408 (Fabian & Ward 1993), NGC 2146 (Armus et al. 1995) and NGC 1569 (Heckman et al. 1995).

Alternatively, for the nuclear source X-1 we may consider a contribution due to photoionization heating by a hidden Seyfert nucleus. Adopting the fitted thermal plasma model as a first approximation, the emission measure is considerably smaller than that of extended X-ray sources in other Seyfert galaxies. For example, the X-ray emission extended over the inner 6 kpc radius in NGC 1068 requires emission measure $\sim 7 \times 10^{64}$ cm^{-3} and electron density $n \sim 0.15$ at an assumed temperature of 10^7 K (Halpern 1992). This medium would be in rough pressure balance with the 'diffuse ionized medium' seen in [N II] and Hα (Bland-Hawthorn, Sokolowski & Cecil 1991). Similarly, Wilson et al. (1992) argued that $(4\text{–}9)\times 10^7$ $M_\odot$ of hot gas would be required to account for the extended *nuclear* X-rays in NGC 1068. In NGC 4151 (Morse et al. 1995), the extended X-ray emission has a luminosity of $\sim 1.7 \times 10^{41}$ erg s^{-1}, which would require a medium of $T \sim 10^7$ K and $n \sim 0.3$ if it were to be in pressure equilibrium with the extended narrow-line region clouds. Both NGC 1068 and NGC 4151 have luminous enough ionizing continua to heat their gas to 10^7 K and render it optically thin to 1 keV X-rays. The required ionization parameter $\xi = L/nr^2$ is ~ 100 for a $\Gamma = 2$ power law. For the case of NGC 1672, taking $n = 0.17$ and $r = 880$ pc requires an ionizing luminosity $L \sim 1 \times 10^{44}$ ergs s^{-1}. This would be a fairly strong Seyfert, and its ionizing luminosity would be comparable to its far-infrared luminosity, although its IRAS *colours* show no evidence for a luminous Seyfert component.

The required intrinsic X-ray luminosity in the Seyfert scenario is about 500 times larger than the 2–10 keV luminosity observed by GINGA, and suggests that if a Seyfert is photoionizing the central region, we are seeing little if any scattered X-ray flux from the nucleus. The properties of X-1 listed in Table 2 allow it to have a Thomson depth of only $\sim 3\times 10^{-4}$, which is not great enough to account for the flux observed by GINGA, although it is roughly compatible with the *soft* X-ray flux being scattered. For either scattering or photoionization heating to account for X-1, the geometry would have to be such as to hide the broad-line region, if any, and the continuum source, but with a relatively large opening angle so as to cause little azimuthal asymmetry in the extended X-ray source, and little reprocessed, warm infrared emission. The existence Seyfert 2 galaxies whose observed X-ray luminosity is even less than 10^{40} erg s^{-1} can perhaps be similarly explained by the lack of a suitable scattering mirror.

3.2 Sources X-2 and X-3

Sources X-2 and X-3 have not been the subjects of detailed studies in the past. Baumgart & Peterson (1986) commented upon vigorous star formation at the ends of NGC 1672's bar seen in near-infrared photographic plates, but did not present quantitative information. Similarly, Hα hotspots at the ends of the bar, as well as along two of the four arms, can be seen in fig. 3 of Sérsic & Calderón (1979), and fig. 2c of SWB96. The abundances seem to be about solar in these regions, and the extinction is $E(B\text{–}V) \approx 0.27$ for both (SWB96). X-2 and X-3 are each over 200 times more luminous in soft X-rays than the R136 nebula of 30 Doradus. Their emission can be modelled by thermal gas emission, although due to their faintness we cannot rigorously rule out a substantial contribution from X-ray binaries.

3.3 An examination of the NGC 1672/NGC 1688 interaction scenario

The 39 arcmin angular separation between NGC 1672 and NGC 1688 corresponds to a separation in the plane of the sky of $\approx$ 260 kiloparsecs. The difference in radial velocities between NGC 1672 and NGC 1688 is about 72 km s^{-1} (Elmegreen et al. 1991). The characteristic separation velocity in the plane of the sky is probably somewhat larger than the radial velocity difference due to geometrical effects (the radial velocities are only one dimensional). In addition, given that a NGC 1672/NGC 1688 interaction took place, the orbital speed will have been larger when NGC 1672 and NGC 1688 were closer together. We estimate that a putative interaction would have happened on the order of 1.5 billion years ago. Since Galactic bars are thought to form on timescales shorter than 1.5 billion years (a few times 10^8 years), this strongly suggests that the starburst activity we see in NGC 1672 is not a direct result of the NGC 1672/NGC 1688 interaction but is rather a more transitory and indirect phenomenon resulting from the nature of the gas flow in the bar.

ACKNOWLEDGMENTS

We acknowledge discussions with D. Calzetti, H. Ebeling, A.C. Fabian, S. Sigurdsson, E. Terlevich, R. Terlevich, M.

Ward and the members of the Institute of Astronomy X-ray group. We thank P.O. Lindblad and S. Jörsäter for kindly sharing some of their results prior to publication. We acknowledge financial support from the United States National Science Foundation and the British Overseas Research Studentship Programme (WNB), NASA grant NAG 5-1935 (JPH) and the JSPC and the British Council (KI). The *ROSAT* project is supported by the Bundesministerium für Forschung und Technologie (BMFT) and the Max-Planck society. Much of our analysis has relied on the ASTERIX and FTOOLS X-ray data processing systems and the XSPEC X-ray spectral fitting software, and we thank the people who have created and maintain this software. This research has made use of the SIMBAD database, operated at CDS, Strasbourg, France and the NASA/IPAC extragalactic database (Helou et al. 1991) which is operated by the Jet Propulsion Laboratory, Caltech.

REFERENCES

Alloin D., Collin-Souffrin S., Joly M., Vigroux L., 1979, A&A, 78, 200
Anders E., Grevesse N., 1989, Geochimica et Cosmochimica Acta, 53, 197
Armus L., Heckman T.M., Weaver K.A., Lehnert M.D., 1995, ApJ, in press
Athanassoula E., 1992, MNRAS, 259, 345
Awaki H., Koyama K., 1993, Adv. Space Res., 13, 221
Baumgart C.W., Peterson C.J., 1986, PASP, 98, 56
Bland-Hawthorn J., Sokolowski J., Cecil G. 1991, ApJ, 375, 78
Bowyer S., Lieu R., Sidher S.D., Lampton M., Knude J., 1995, Nature, 375, 212
Brindle C., Hough J.H., Bailey J.A., Axon D.J., Ward M.J., Sparks W.B., McLean I.S., 1990, MNRAS, 244, 577
Brinkmann W. et al., 1994, A&A, 288, 433
Burstein D., Heiles C., 1978, ApJ, 225, 40
Calzetti D., Kinney A.L., Storchi-Bergmann T., 1994, ApJ, 429, 582
David L.P., Jones C., Forman W., 1992, ApJ, 388, 82
David L.P., Harnden F.R., Kearns K.E., Zombeck M.V., 1995, The ROSAT High Resolution Imager. GSFC, Greenbelt
Davies R.D., 1989, QJRAS, 30, 295
de Vaucouleurs G., 1975, in Sandage A., Sandage M., Kristian J., eds, Galaxies and the Universe, Univ. of Chicago Press, Chicago, p. 557
Díaz A.I., 1985, PhD thesis, University of Sussex
Elmegreem D.M., Sundin M., Elmegreen B., Sundelius B., 1991, A&A, 244, 52
Fabian A.C., Ward M.J., 1993, MNRAS, 263, 51P
Fabbiano G., 1988, ApJ, 330, 672
Fabbiano G., Feigelson E., Zamorani G., 1982, ApJ, 256, 397
Fabbiano G., Kim D.-W., Trinchieri G., 1992, ApJS, 80, 531
Forbes D.A., Ward M.J., DePoy D.L., Boisson C., Smith M.S., 1992, MNRAS, 254, 509
García-Vargas M.L., Díaz A.I., Terlevich R.J., Terlevich E., 1990, Astr. Space Sci., 171, 65
Griffiths R.E., Feigelson E., van Speybroeck L., 1979, Bull. Am. Ast. Soc., 11, 466
Halpern J., 1992, in Holt S.S., Neff S.G., Urry C.M., eds, Testing the AGN Paradigm. AIP Press, New York, p. 524
Harnden F.R., et al., 1979, ApJ, 234, L51
Harnett J.I., 1987, MNRAS, 227, 887
Hasinger G., Turner T.J., George I.M., Boese G., 1992, Legacy #2, The Journal of the High Energy Astrophysics Science Archive Research Center, NASA/GSFC
Heckman T.M., Armus L., Miley G.K., 1990, ApJS, 74, 833
Heckman T.M., Dahlem M., Lehnert M.D., Fabbiano G., Gilmore D., Waller W.H., 1995, ApJ, 448, 138
Helou G., Madore B.F., Schmitz M., Bicay M.D., Wu X., Bennett J., 1991, in Egret D., Albrecht M., eds, Databases and On-Line Data in Astronomy, Kluwer, Dordrecht, p. 89
Iwasawa K., Yaqoob T., Awaki H., Ogasaka Y., 1994, PASJ, 46, L167
Kawara K., Nishida M., Gregory B., 1987, ApJ, 321, L35
Kinney A.L., Bohlin R.C., Calzetti D., Panagia N., Wyse R.F.G., 1993, ApJS, 86, 5
Kruper J.S., Urry C.M., Canizares C.R., 1990, ApJS, 74, 347
Lampton M., Margon B., Bowyer S., 1976, ApJ, 208, 177
Lasker B.M., Sturch C.R., McLean B.J., Russell J.L., Jenkner H., Shara M.M., 1990, AJ, 99, 2019
Leene A., Cox P., 1987, A&A, 174, L1
Lequeux J., 1988, in Bailey M.E., Williams D.A., eds, Dust in the Universe, Cambridge Univ. Press, Cambridge, p. 449
Lindblad P.O., Jörsäter S., 1996, A&A, in preparation
MacLow M.-M., McCray R. 1988, ApJ, 324, 776
Maia M., Pastoriza M., Bica E., Dottori H., 1994, ApJS, 93, 425
Mathewson D.S., Rome J.M., 1963, Aust J Phys, 16, 360
Mathis J.S., 1990, ARA&A, 28, 37
Moorwood A.F.M., Oliva E., 1988, A&A, 203, 278
Morse J.A., 1994, PASP, 106, 675
Morse J.A., Wilson A.S., Elvis M., Weaver K.A., 1995, ApJ, 439, 121
Osmer P.S., Smith M.G., Weedman D.W., 1974, ApJ, 192, 279 (OSW74)
Pastoriza M.G., 1973, PhD thesis, Córdoba Instituto de Matemáticas, Astronomía y Física
Pfeffermann E. et al., 1987, Proc. SPIE, 733, 519
Press W.H., Flannery B.P., Teukolsky S.A., Vetterling W.T., 1989, Numerical Recipes in Pascal. Cambridge Univ. Press, Cambridge
Rangarajan F.V.N., White D.A., Ebeling H., Fabian A.C., 1995, MNRAS, submitted
Rosa M.R., Benvenuti P., 1995, A&A, in press
Sandage A., Bedke J., 1994, The Carnegie Atlas of Galaxies. CIOW Press, Washington D.C.
Sanders D.B., Soifer B.T., Elias J.H., Neugebauer G., Matthews K., 1988, ApJ, 328, L35
Sandqvist Aa., Jörsäter S., Lindblad P.O., 1995, A&A, 295, 585
Sérsic J.L., 1968, Atlas de Galaxias Australes. Córdoba Univ. Press, Córdoba
Sérsic J.L., Pastoriza M., 1965, PASP, 77, 287
Sérsic J.L., Calderón J.H., 1979, Ast. and Space Sci., 62, 211
Shafer R.A., Haberl F., Arnaud K.A., Tennant A.F., 1991, XSPEC Users Guide. ESA Publications, Noordwijk
Storchi-Bergmann T., Calzetti D., Kinney A.L., 1994, ApJ, 429, 572
Storchi-Bergmann T., Wilson, A.S., Baldwin, J.A., 1996, ApJ, in press (SWB96)
Tielens A.G.G.M., Allamandola L.J., 1987, in Hollenbach D.J., Thronson H.A., eds, Interstellar Processes, Reidel, Dordrecht, p. 397
Tovmassian H.M., 1966, Aust J Phys, 19, 883
Tovmassian H.M., 1968, The Observatory, 88, 227
Trümper J., 1983, Adv. Space Res., 4, 241
Turner T.J., George I.M., Mushotzky R.F., 1993, ApJ, 412, 72
Ulvestad J.S., Wilson A.S., 1984, ApJ, 285, 439
Véron M.P., Véron P., Zuiderwijk E.J., 1981, A&A, 98, 34
Wang Q., Helfand D.J., 1991, ApJ, 370, 541
Ward M.J., 1988, MNRAS, 231, 1P
Wilson A.S., Elvis M., Lawrence A., Bland-Hawthorn J., 1992, ApJ, 391, L75
Witt A.N., Thronson H.A., Capuano J.M., 1992, ApJ, 393, 611